

# Contrastive Conformal Sets

Yahya Alkhatib<sup>1</sup>

Wee Peng Tay<sup>1</sup>

<sup>1</sup>School of Electrical and Electronic Engineering, Nanyang Technological University, Singapore

## Abstract

Contrastive learning produces coherent semantic feature embeddings by encouraging positive samples to cluster closely while separating negative samples. However, existing contrastive learning methods lack principled guarantees on coverage within the semantic feature space. We extend conformal prediction to this setting by introducing minimum-volume covering sets equipped with learnable generalized multi-norm constraints. We propose a method that constructs conformal sets guaranteeing user-specified coverage of positive samples while maximizing negative sample exclusion. We establish theoretically that volume minimization serves as a proxy for negative exclusion, enabling our approach to operate effectively even when negative pairs are unavailable. The positive inclusion guarantee inherits the distribution-free coverage property of conformal prediction, while negative exclusion is maximized through learned set geometry optimized on a held-out training split. Experiments on simulated and real-world image datasets demonstrate improved inclusion-exclusion trade-offs compared to standard distance-based conformal baselines.

## 1 INTRODUCTION

Effective machine learning fundamentally relies on learning embeddings that capture semantic relationships between data samples [Boser et al., 1992, Dinh et al., 2025, Wen et al., 2016, Schroff et al., 2015]. In high-dimensional feature spaces, this objective is formalized as placing semantically similar samples in proximity while distributing dissimilar samples to distinct regions. Contrastive learning provides a principled framework for achieving this goal by training encoders to minimize distances to similar samples (positive

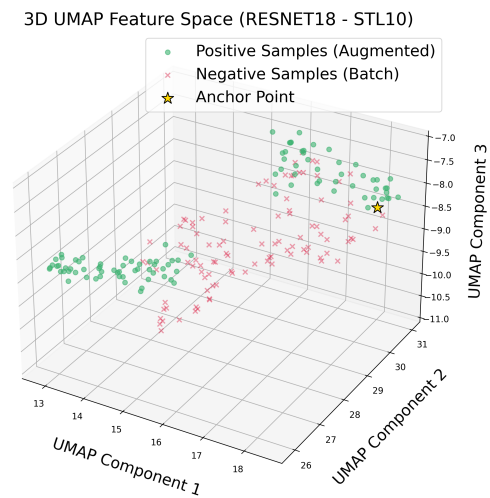


Figure 1: 3D UMAP projection of the semantic features of an STL10 anchor point and its positive and negative samples.

pairs) while maximizing distances to dissimilar samples (negative pairs) under an appropriate embedding metric [Chen et al., 2020, van den Oord et al., 2018, Zhu et al., 2020, Shi et al., 2023]. A key strength of contrastive learning is its applicability to both supervised settings, where similarity is defined by labels, and unsupervised settings, where positive and/or negative pairs are generated through data augmentation [Zhu et al., 2020]. This flexibility has established contrastive learning as a dominant paradigm for pretraining transferable representations that achieve strong performance across diverse downstream tasks [Ardehshir and Azizan, 2022]. In high-stakes domains such as healthcare and finance, there is an increasing demand for models that provide rigorous and principled quantification of uncertainty, rather than relying on heuristic measures. This challenge is particularly pronounced in high-dimensional semantic embedding spaces, where point estimates lack guarantees of reliability.

Despite the widespread adoption of contrastive learning across numerous applications, there remains a lack of systematic methodologies for certifying a model’s ability to cluster semantically similar examples within a user-specified tolerance level. For instance, Fig. 1 depicts a UMAP projection [McInnes et al., 2018] of the semantic features of an input image, generated by a trained unsupervised contrastive model, in  $\mathbb{R}^3$ . Quantifying the model’s uncertainty in distinguishing the input from its corresponding positive and negative samples in such a setting is inherently challenging. Notably, as a mapping from the input space to the semantic feature space, the performance of such models is typically assessed based on downstream tasks.

A natural question, then, is whether one can evaluate the uncertainty of the encoder as a standalone projector to the semantic space, independent of any downstream application. Such an intrinsic characterization of embedding quality is valuable for two key reasons. First, it serves as a diagnostic tool for model selection and hyperparameter optimization, enabling practitioners to compare projectors based on the tightness of their covering sets at a fixed coverage level, without relying on specific downstream tasks. Second, it establishes a principled foundation for subsequent applications—such as out-of-distribution (OOD) detection or retrieval systems—which can leverage the certified embedding neighbourhoods and inherit their coverage guarantees.

Some works have considered uncertainty quantification for contrastive learners, primarily by replacing deterministic embeddings with stochastic distributions [Oh et al., 2019] or aggregating Gaussian mappings to derive a scalar uncertainty measure from covariance norms [Wu and Goodman, 2020]. Similarly, contrastive representations have been leveraged for OOD detection using Mahalanobis distances on intermediate features [Winkens et al., 2020], novelty scores derived from shifted augmentations [Tack et al., 2020], and energy-based discriminative-generative models [Liu and Abbeel, 2020]. A common thread across all of these methods is that they provide *heuristic* measures of embedding uncertainty—whether through learned variances, covariance norms, Mahalanobis distances, or energy-based scores—without yielding certified spatial regions. While these approaches effectively summarize uncertainty into scalar or distributional scores, they fundamentally lack the geometric structure required to provide formal, user-specified inclusion guarantees for positive samples.

To address this gap, we aim to construct sets in the semantic feature space that include the embeddings of positive samples with a user-specified probability of at least  $1 - \alpha$ , while simultaneously maximizing the exclusion of negative samples. This is inspired by the framework of conformal prediction (CP), a principled approach to uncertainty quantification that offers strong theoretical guarantees and broad applicability [Vovk et al., 2005, Angelopoulos and Bates, 2022, Angelopoulos et al., 2025, Shafer and Vovk, 2008,

Messoudi et al., 2020, Quach et al., 2024, Foygel Barber et al., 2023, Lei et al., 2015]. CP has traditionally been applied to quantify uncertainty in the output space, producing prediction sets that contain the true label with a user-specified coverage guarantee in a distribution-free and model-agnostic manner. This property makes CP a versatile tool for uncertainty quantification, as it treats the underlying model as a black box [Angelopoulos and Bates, 2022, Angelopoulos et al., 2025]. Recent advancements have extended CP to leverage semantic feature space information; for example, Teng et al. [2023] utilize learned representations to improve the efficiency of output-space prediction sets, though the resulting sets remain in the output space rather than the feature space. While prior work has explored CP with multi-valued scoring functions and in output spaces [Messoudi et al., 2020, Klein et al., 2025, Diquigiovanni et al., 2022], the direct construction of CP sets within the semantic feature space remains largely uncharted.

In this work, we propose a framework that addresses this challenge. The positive inclusion guarantee is derived from the distribution-free coverage property of CP, achieved through a calibration-quantile threshold, while negative exclusion is optimized by learning the geometry of the covering set via generalized multi-norm constraints and scaling matrices. We further establish, both theoretically and empirically, that minimizing the volume of these sets serves as a principled proxy for maximizing negative exclusion, enabling the framework to construct discriminative boundaries even when only positive samples are available. The proposed sets are constructed as overlays on the existing embedding space, leaving the learned representations unaltered, and can serve as a foundation for downstream tasks such as OOD detection.

Our main contributions are as follows:

1. We introduce *contrastive conformal sets*: a framework for constructing conformal prediction sets directly in the semantic feature space around anchor embeddings, designed to include positive samples while excluding negative samples.
2. We show that positive inclusion inherits the distribution-free coverage guarantee of conformal prediction at any user-specified level, while the set geometry is optimized to maximize negative exclusion through learnable norm exponents and scaling parameters.
3. We establish that, within a nested family of covering sets, minimum-volume sets maximize negative exclusion (Proposition 1), providing a principled proxy objective when only positive samples are available—a common setting in contrastive learning.
4. We validate the framework empirically on simulated and real-world image benchmarks, demonstrating that it achieves the prescribed positive coverage while sub-

stantially improving negative exclusion over vanilla conformal baselines. We further show that the learned covering sets yield competitive or superior performance on OOD detection against several dedicated methods.

## 2 PRELIMINARIES

We begin by reviewing the standard split CP framework, which constructs prediction sets in the output space. This serves as a foundation for several concepts that will be extended in our work.

**Set-Valued Predictors and Nonconformity Scores.** The goal of CP is to construct a set-valued mapping  $\mathcal{C} : \mathcal{X} \rightarrow 2^{\mathcal{Y}}$  that provides uncertainty quantification for model predictions. The quality of such a mapping is assessed along two key dimensions: statistical validity (coverage) and practical utility (efficiency).

CP constructs prediction sets by leveraging nonconformity scores, which quantify the degree to which a candidate label  $Y$  conforms to the model’s prediction. Given a pre-trained model  $f_\theta$ , the nonconformity score for an input-label pair  $(X, Y)$  is defined as  $s(X, Y; \theta) = L(f_\theta(X), Y)$ , where  $L$  is a task-specific discrepancy measure (e.g. the softmax probability of  $Y$  given  $X$ ).

Given a threshold  $t \in \mathbb{R}$ , the prediction set is constructed by including all candidate labels whose nonconformity scores do not exceed the threshold:

$$\mathcal{C}_{\theta,t}(X) = \{y : s(X, y; \theta) \leq t\}. \quad (1)$$

**The Split Conformal Guarantee.** To ensure that the prediction set achieves a user-specified coverage level  $1 - \alpha$ , the split CP framework employs a distribution-free calibration procedure. The dataset is partitioned into three disjoint subsets: a training set  $\mathcal{D}$  (used to train  $f_\theta$ ), a calibration set  $\mathcal{D}_{\text{cal}}$  of size  $n_{\text{cal}}$ , and a test set  $\mathcal{D}_{\text{test}}$ .

Nonconformity scores are computed for all instances in  $\mathcal{D}_{\text{cal}}$ , and the critical threshold  $t = \hat{q}_\alpha$  is chosen as the empirical  $[(1 - \alpha)(n_{\text{cal}} + 1)]/n_{\text{cal}}$  quantile of these scores. Assuming that the calibration and test data are exchangeable—a property typically satisfied by random splitting—this threshold guarantees marginal coverage for any test point  $(X, Y) \in \mathcal{D}_{\text{test}}$  [Shafer and Vovk, 2008, Foygel Barber et al., 2023, Angelopoulos and Bates, 2022]:

$$\mathbb{P}(Y \in \mathcal{C}_{\theta, \hat{q}_\alpha}(X)) = \mathbb{P}(s(X, Y; \theta) \leq \hat{q}_\alpha) \geq 1 - \alpha. \quad (2)$$

This probability is taken jointly over the randomness of the calibration data and the test point.

Building on these foundations, the next section introduces our problem formulation: extending CP to the semantic

feature space of models, with a focus on constructing contrastive sets that simultaneously optimize for the inclusion of positive samples and the exclusion of negative samples. We defer all proofs to Appendix A.

## 3 PROBLEM STATEMENT

**Positive and Negative Samples.** Let  $\mathcal{X}$  denote the input space and  $\mathcal{Y}$  the label space, with  $(X, Y)$  representing a pair of random variables distributed according to the joint probability density function (pdf)  $p_{X,Y}$ . For a given anchor realization  $(X = x_0, Y = y_0)$ , the oracle distributions for generating positive and negative samples are defined as follows:

$$p_{\text{pos}}^*(\cdot) \propto p_{X,Y}(\cdot, y = y_0), \quad (3)$$

$$p_{\text{neg}}^*(\cdot) \propto \int_{\{y \neq y_0\}} p_{X,Y}(\cdot, y) dy, \quad (4)$$

where  $p_{\text{pos}}^*$  generates samples conditioned on the same label as the anchor, and  $p_{\text{neg}}^*$  generates samples conditioned on labels different from that of the anchor.

In supervised settings, where label information is available [Khosla et al., 2020], these oracle distributions are well-defined and training samples are accessible. However, in unsupervised settings, where labels are unavailable [Saunshi et al., 2019], the oracle mechanisms  $p_{\text{pos}}^*$  and  $p_{\text{neg}}^*$  cannot be directly accessed. Instead, practitioners approximate these distributions using conditional mechanisms  $p_{\text{pos}}(\cdot | X = x_0)$  and  $p_{\text{neg}}(\cdot | X = x_0)$ , respectively. The design of these approximations aims to closely align with the oracle distributions, a key desideratum in contrastive learning that has motivated extensive research [Saunshi et al., 2019, Chuang et al., 2020, Khosla et al., 2020].

While the design of these approximations is an important challenge, it is not the primary focus of this work. Instead, our objective is to develop a principled framework for constructing *contrastive conformal sets* that provide rigorous guarantees for *any given contrastive learning model*. Specifically, we aim to ensure that the embeddings of positive samples lie within a well-defined neighbourhood of the anchor embedding with high probability. Our framework also provides the option of updating the contrastive learning model weights to achieve better inclusion-exclusion trade-offs, leading to more robust contrastive embeddings.

**Contrastive Conformal Learning Objective.** The primary objective of this work is to certify embedding neighbourhoods within a semantic feature space  $\mathcal{Z}$  equipped with a metric  $g$ . Let  $\mathcal{D}$  denote a dataset of anchor points  $X \in \mathcal{X}$ . For any given anchor  $X$ , let  $\mathcal{X}_{\text{pos}}, \mathcal{X}_{\text{neg}} \subset \mathcal{X}$  define the subsets of its associated positive and negative samples, respectively; these associations may be established through unsupervised augmentations or supervised labels  $Y \in \mathcal{Y}$ .

Consider an encoder  $\theta : \mathcal{X} \rightarrow \mathcal{Z}$ , pretrained on  $\mathcal{D}$ , that maps an input to its corresponding embedding  $Z = \theta(X)$ . A well-trained encoder is expected to map positive samples to embeddings that are proximal to the anchor’s embedding, while pushing the embeddings of negative samples sufficiently far away.

Formally, for a given threshold  $t > 0$ , the neighbourhood of an embedding  $Z$  is defined as:

$$\mathcal{N}(Z) \triangleq \{z \in \mathcal{Z} : g(Z, z) \leq t\}, \quad (5)$$

where  $g : \mathcal{Z} \times \mathcal{Z} \rightarrow \mathbb{R}_+$  is a distance metric that quantifies the proximity between embeddings. The choice of  $g$  and  $t$  determines the geometry of the neighbourhood  $\mathcal{N}(Z)$ . An ideal encoder satisfies two key properties: (i) the embedding of any positive sample lies within the neighbourhood,  $Z_{\text{pos}} \in \mathcal{N}(Z)$ , and (ii) the embedding of any negative sample lies outside the neighbourhood,  $g(Z, Z_{\text{neg}}) > t$ .

In practice, these properties cannot be enforced deterministically. Instead, the goal is to construct  $\mathcal{N}(Z)$  such that the embeddings of positive samples are included with high probability, controlled by a user-specified tolerance level  $\alpha \in (0, 1)$ , while simultaneously maximizing the probability of excluding negative embeddings. This leads to the following optimization problem:

$$\arg \max_{\mathcal{N}} \mathbb{P}(Z_{\text{neg}} \notin \mathcal{N}(Z)) \quad (6a)$$

$$\text{s. t. } \mathbb{P}(Z_{\text{pos}} \in \mathcal{N}(Z)) \geq 1 - \alpha. \quad (6b)$$

The objective is to determine the metric  $g$  and the threshold  $t$  that define  $\mathcal{N}(Z)$ , ensuring that the positive inclusion constraint in (6b) is satisfied at the desired coverage level, while maximizing the negative exclusion probability in (6a). The optimal set  $\mathcal{N}(Z)$  can then be used in downstream applications, such as OOD detection, where the inclusion of positive samples and exclusion of negative samples are critical for performance.

**Corollary 1** (Oracle Inclusion-Exclusion Bounds). *If the positive inclusion condition in (6b) is satisfied by some positive generation mechanism  $p_{\text{pos}}$  at level  $1 - \alpha$ , and the negative exclusion probability in (6a) is bounded below by  $1 - \beta$  for some  $\beta \in (0, 1)$ , then the oracle mechanisms  $p_{\text{pos}}^*$  and  $p_{\text{neg}}^*$  satisfy positive inclusion and negative exclusion levels bounded below by*

$$1 - \frac{\alpha}{\mathbb{P}(Y_{\text{pos}} = Y)} \quad \text{and} \quad 1 - \frac{\beta}{\mathbb{P}(Y_{\text{neg}} \neq Y)}, \quad (7)$$

respectively. Here,  $Y_{\text{pos}}$  and  $Y_{\text{neg}}$  are the labels of the positive and negative samples, respectively, and  $Y$  is the label of the anchor.

This highlights a fundamental principle of contrastive learning: the closer the alignment between the generation mechanisms  $p_{\text{pos}}$ ,  $p_{\text{neg}}$  and their respective oracle distributions

$p_{\text{pos}}^*$ ,  $p_{\text{neg}}^*$ —specifically, the more accurately  $X_{\text{pos}}$  represents a sample from the same class as  $X$  and  $X_{\text{neg}}$  represents a sample from a different class—the stronger the empirical guarantees for inclusion and exclusion.

## 4 METHODOLOGY

To address this problem, we begin by constructing covering sets inspired by the principles of CP. Let  $\mathcal{D}_{\text{cal}}$  denote a held-out calibration set, where each sample is represented as a triplet  $(X, X_{\text{pos}}, X_{\text{neg}})$ . Here,  $X$  serves as the anchor,  $X_{\text{pos}}$  is a positive sample drawn from the conditional distribution  $p_{\text{pos}}(\cdot | X)$ , and  $X_{\text{neg}}$  is a negative sample drawn from  $p_{\text{neg}}(\cdot | X)$ . In Section 4.3, we extend this framework to scenarios where only positive samples  $X_{\text{pos}}$  are available.

For each calibration triplet, the pretrained encoder  $\theta$  maps the input features into the semantic feature space  $\mathcal{Z}$ . Using a chosen distance function  $s(\cdot, \cdot)$ , we compute the distance  $s(Z, Z_{\text{pos}})$  between the anchor’s embedding and its conditionally generated positive counterpart.

**Lemma 1** (Positive Inclusion Guarantee). *Suppose  $\mathcal{D}_{\text{cal}}$  consists of  $n_{\text{cal}}$  samples whose anchors  $X^j$  and their corresponding positive samples  $X_{\text{pos}}^j$  are projected to embeddings  $Z^j, Z_{\text{pos}}^j$ , respectively, for  $j = 1, \dots, n_{\text{cal}}$ . Suppose the test anchor  $X$  is projected to  $Z$ , and its positive sample  $X_{\text{pos}}$  is projected to  $Z_{\text{pos}}$ . Assuming that  $X$  and the anchors  $X^j$  for  $j = 1, \dots, n_{\text{cal}}$  are exchangeable given the training set  $\mathcal{D}$ , the distance  $s(Z, Z_{\text{pos}})$  from the test anchor to its positive sample satisfies*

$$\mathbb{P}(s(Z, Z_{\text{pos}}) \leq \hat{q}_\alpha) \geq 1 - \alpha, \quad (8)$$

where  $\hat{q}_\alpha$  is the  $\lceil (1 - \alpha)(n_{\text{cal}} + 1) \rceil$ -th smallest value of the calibration positive distance scores,  $\{s(Z^j, Z_{\text{pos}}^j)\}_{j=1}^{n_{\text{cal}}}$ . The probability is taken marginally over the joint distribution of the calibration data and the test point.

In the Euclidean space  $\mathbb{R}^d$ , two common choices for any pair of vectors  $u, v \in \mathbb{R}^d$  are the  $\ell_2$  distance and the Mahalanobis distance:

$$s_{\ell_2}(u, v) = \|u - v\|_2, \quad (9)$$

$$s_{\text{Mah}}(u, v) = \sqrt{(u - v)^\top \Sigma^{-1} (u - v)}. \quad (10)$$

To avoid introducing bias, the covariance matrix  $\Sigma$  in  $s_{\text{Mah}}$  must be estimated from a held-out split of data disjoint from  $\mathcal{D}_{\text{cal}}$  [Johnstone and Cox, 2021]. Geometrically,  $s_{\ell_2}$  yields a fixed-radius hyper-ball in the embedding space, whereas  $s_{\text{Mah}}$  produces a hyper-ellipsoid whose shape is governed by the covariance structure of the data.

Lemma 1 guarantees the positive inclusion requirement in (6b). However, fixing the scoring function  $s(Z, \cdot)$  provides no direct control over the negative exclusion objective in (6a); the exclusion probability depends entirely on how the

calibration negative scores are distributed relative to the positive scores. To address this, we propose a learnable adaptive scoring function that dynamically adjusts the geometry of the conformal set to maximize the exclusion of negative samples while maintaining the desired positive inclusion rate. By parameterizing the score with learnable components, such as scaling matrices and norm exponents, we enable the conformal set to adapt to the underlying data distribution. This approach ensures that the positive inclusion constraint in (6b) is satisfied, while the negative exclusion probability in (6a) is optimized through a data-driven learning process.

#### 4.1 LEARNABLE-METRIC CONFORMAL SETS

To simultaneously satisfy the positive inclusion constraint in (6b) and maximize the negative exclusion probability in (6a), we require covering sets whose geometry can adapt to the distribution of semantic features.

**Single-norm covering sets.** We define a family of candidate sets around an anchor embedding  $Z$ , parameterized by a learnable exponent  $p > 0$  and a scaling matrix  $M \in \mathbb{R}^{d \times d}$ :

$$\mathcal{N}(Z) = \{z : \|M(Z - z)\|_p \leq t\}, \quad (11)$$

for a threshold  $t > 0$ . When  $p \geq 1$ , the resulting set is convex and smooth; when  $p < 1$ , it becomes increasingly anisotropic, offering greater flexibility to match non-standard feature distributions. The volume of this set can be expressed in closed form as

$$\text{Vol}(\mathcal{N}) = \lambda(\mathbb{B}_{\|\cdot\|_p}(t)) \cdot \det(M)^{-1}, \quad (12)$$

where  $\lambda(\cdot)$  denotes the Lebesgue measure. For the  $\ell_p$ -ball of radius  $t$ , this takes the explicit form

$$\lambda(\mathbb{B}_{\|\cdot\|_p}(t)) = \frac{(2t)^d \Gamma(1 + \frac{1}{p})^d}{\Gamma(1 + \frac{d}{p})} = t^d \lambda(\mathbb{B}_{\|\cdot\|_p}(1)),$$

where  $\Gamma(\cdot)$  is the gamma function and  $\mathbb{B}_{\|\cdot\|_p}(1)$  is the unit  $p$ -norm ball [Braun et al., 2025].

**Generalized multi-norm covering sets.** Although a learnable norm and scaling matrix provide considerable expressive power, semantic features may exhibit heterogeneous distributional shapes along different coordinate directions. To accommodate this, we adopt a generalized hyper-ball construction [Wang, 2005], in which each dimension is endowed with its own exponent:

$$\mathcal{N}(Z) = \left\{ z : \sum_{j=1}^d m_j^{p_j} \cdot |\{Z - z\}_j|^{p_j} \leq t \right\}, \quad (13)$$

where  $\{a\}_j$  denotes the  $j$ -th component of the vector  $a$ , each  $m_j > 0$  is a learnable scale parameter, and each

$p_j > 0$  is a learnable exponent. We can construct learnable vectors of them such that  $p = [p_1, p_2, \dots, p_d]^\top$  and  $m = [m_1, m_2, \dots, m_d]^\top$ . Following [Wang, 2005], the volume of this generalized set admits the closed-form expression

$$\text{Vol}(\mathcal{N}) = \frac{t^{\sum_{j=1}^d 1/p_j}}{\prod_{j=1}^d m_j} \cdot \frac{2^d \prod_{j=1}^d \Gamma(1 + \frac{1}{p_j})}{\Gamma(1 + \sum_{j=1}^d \frac{1}{p_j})}. \quad (14)$$

With these set constructions, we are now ready to tackle the objective of constructing covering sets that include positive samples with user-specified tolerance and maximum exclusion of negative samples.

#### 4.2 OPTIMIZATION OBJECTIVE

Let  $\mathcal{D}_{\text{train}}$  denote a training set of size  $n_{\text{train}}$  (not to be confused with  $\mathcal{D}$ , the data used to pretrain the encoder  $\theta(\cdot)$ ). To approximate the probabilities in (6a) and (6b), we reformulate the optimization problem as follows:

$$\arg \max_{M,p} \frac{1}{n_{\text{train}}} \sum_{i=1}^{n_{\text{train}}} \mathbf{1}_{\{g_{M,p}(Z_{\text{neg}}^i, Z^i) > t\}}, \quad (15a)$$

$$\text{s. t. } \frac{1}{n_{\text{train}}} \sum_{i=1}^{n_{\text{train}}} \mathbf{1}_{\{g_{M,p}(Z_{\text{pos}}^i, Z^i) \leq t\}} \geq 1 - \alpha, \quad (15b)$$

where  $g_{M,p}(\cdot, Z)$  represents either the single-norm metric or the generalized multi-norm metric, and the superscript  $i$  indexes individual instances. To enable optimization via first-order methods, we introduce the following modifications:

1. The threshold  $t$  is set to the empirical  $\lceil(1 - \alpha)(n_{\text{train}} + 1)\rceil/n_{\text{train}}$  quantile of the positive distances  $g_{M,p}(Z_{\text{pos}}, Z)$  at each iteration, denoted as  $\hat{q}_\alpha$ . This ensures that the constraint in (15b) is satisfied implicitly by Lemma 1. Since the quantile computation involves a sorting operation, which is non-differentiable,  $\hat{q}_\alpha$  is detached from the computational graph during the backward pass.
2. The non-differentiable indicator function  $\mathbf{1}_{\{c > t\}}$  is replaced with a smooth sigmoid approximation, defined as  $\sigma_T(c - t) = \frac{1}{1 + e^{-\frac{1}{T}(c-t)}}$ , where  $T$  is a temperature parameter. Increasing  $T$  improves the sharpness of the approximation but may lead to vanishing gradients.
3. To enforce positivity constraints on the parameters without resorting to constrained optimization solvers, we optimize over the element-wise absolute values  $|m|$  and  $|p|$  for the generalized multi-norm metric. For the single-norm metric, we parameterize  $M$  as  $M = AA^\top$ , where  $A$  is a learnable matrix. This ensures that  $M$  remains positive semi-definite throughout the optimization process.

The relaxed optimization problem reduces to:

$$\arg \max_{M,p} J_{\text{neg}} \triangleq \frac{1}{n_{\text{train}}} \sum_{i=1}^{n_{\text{train}}} \sigma_T(g_{M,p}(Z_{\text{neg}}^i, Z^i) - \hat{q}_\alpha). \quad (16)$$

This objective directly focuses on maximizing the exclusion of negative samples. However, relying exclusively on this formulation assumes the ready availability of negative pairs, which is not always guaranteed. Furthermore, to be practically informative, the resulting conformal sets must be structurally efficient, i.e., possessing a small Lebesgue measure.

### 4.3 POSITIVE-SAMPLE-ONLY MINIMUM VOLUME SETS

In many modern representation learning frameworks, accessing explicit negative samples can be challenging or architecturally unsupported. Under such positive-sample-only regimes, we must still construct conformal sets that achieve high negative exclusion without directly optimizing against negative instances.

Fortunately, the geometric size of the covering set serves as a theoretically grounded proxy. The following proposition demonstrates that among all nested sets satisfying the positive inclusion constraint in (6b), the one with the smallest volume maximizes the empirical exclusion rate of the negative distribution.

**Proposition 1.** *Let  $\text{Vol}$  denote the reference volume measure on  $\mathcal{Z}$ . Fix  $\alpha \in (0, 1)$  and consider a family of measurable sets*

$$\{\mathcal{B}_t : t \in T\}, \quad \mathcal{B}_t \subseteq \mathcal{Z}, \quad (17)$$

that is nested in  $t$ , i.e.,

$$t_1 \leq t_2 \Rightarrow \mathcal{B}_{t_1} \subseteq \mathcal{B}_{t_2} \text{ and } \text{Vol}(\mathcal{B}_{t_1}) \leq \text{Vol}(\mathcal{B}_{t_2}).$$

Denote by  $Z_{\text{pos}} = \theta(X_{\text{pos}})$  the embedding of positive samples. Let

$$t^* \in \arg \min_{t \in T} \{\text{Vol}(\mathcal{B}_t) : \mathbb{P}(Z_{\text{pos}} \in \mathcal{B}_t) \geq 1 - \alpha\}, \quad (18)$$

and set  $\mathcal{B}_\alpha^* \triangleq \mathcal{B}_{t^*}$ . Then  $\mathcal{B}_\alpha^*$  satisfies the positive inclusion requirement (6b) and maximizes the negative exclusion probability (6a) within the family  $\{\mathcal{B}_t : t \in T\}$ . Equivalently,  $\mathcal{B}_\alpha^*$  is a minimum-volume set in this family among all sets that satisfy (6b).

We call such a set  $\mathcal{B}_\alpha^*$  a *Minimum-Volume  $\alpha$ -Inclusion Set (MV $\alpha$ IS)*.

Guided by Proposition 1, we can bypass the need for negative samples by isolating the volume as our primary minimization objective:

$$\arg \min_{M,p} J_{\text{vol}} \triangleq \frac{1}{n_{\text{train}}} \sum_{i=1}^{n_{\text{train}}} \log \text{Vol}(\mathcal{N}_{\hat{q}_\alpha}(Z^i)), \quad (19)$$

where the threshold  $\hat{q}_\alpha$  is implicitly tied to the empirical  $\lceil (1 - \alpha)(n_{\text{train}} + 1) \rceil / n_{\text{train}}$ -quantile of the positive distances at each iteration, satisfying the inclusion constraint by design.

On the other hand, when negative samples are fully available, the log-volume acts as a potent geometric regularizer alongside the direct exclusion objective. Utilizing the log-volume rather than the raw Lebesgue measure ensures numerical stability against the  $[0, 1]$  bounded sigmoid term. The combined objective becomes:

$$\arg \max_{M,p} J_{\text{neg+vol}} \triangleq \frac{1}{n_{\text{train}}} \sum_{i=1}^{n_{\text{train}}} \left[ (1 - \lambda) \sigma_T(g_{M,p}(Z_{\text{neg}}^i, Z^i) - \hat{q}_\alpha) - \lambda \log \text{Vol}(\mathcal{N}_{\hat{q}_\alpha}(Z^i)) \right], \quad (20)$$

where  $\lambda \in [0, 1]$  is a regularization constant. By controlling  $\lambda$ , we can learn covering sets that strictly minimize the volume, strictly maximize the negative exclusion rate, or smoothly balance both. Notice that setting  $\lambda = 1$  gracefully recovers the positive-sample-only objective  $J_{\text{vol}}$  (formulated equivalently as a maximization of the negative log-volume).

To further enhance the adaptability of the contrastive conformal sets, we propose incorporating the model weights into the optimization process. This approach allows the feature space to dynamically adjust in conjunction with the learned metrics. In practice, contrastive models are often trained using the InfoNCE loss [van den Oord et al., 2018], which is defined as:

$$L_{\text{InfoNCE}} = -\log \frac{e^{\text{sim}(Z, Z_{\text{pos}})/\tau}}{e^{\text{sim}(Z, Z_{\text{pos}})/\tau} + \sum_{Z_{\text{neg}}} e^{\text{sim}(Z, Z_{\text{neg}})/\tau}}, \quad (21)$$

where  $\text{sim}(u, v)$  denotes a similarity measure between  $u$  and  $v$  (commonly the cosine similarity,  $\text{sim}(u, v) = u^\top v$ ), and  $\tau$  is a temperature parameter.

To integrate this into our framework, we augment the optimization objective by including the InfoNCE loss as a regularization term. The resulting objective is given by:

$$\arg \max_{M,p,\theta} J_{\text{neg+vol}} - \lambda_{\text{InfoNCE}} L_{\text{InfoNCE},\theta}, \quad (22)$$

where  $\theta$  represents the model's weights or a selected subset thereof, and  $\lambda_{\text{InfoNCE}}$  is a hyperparameter. This formulation enables the simultaneous optimization of the contrastive

conformal set geometry and the underlying feature representations, thereby improving the alignment of the embedding space with the desired inclusion-exclusion properties.

To guarantee the positive inclusion rate as in (6b), we use a held-out calibration set  $\mathcal{D}_{\text{cal}}$  to find the definitive threshold  $\hat{q}_\alpha$  using the learned metric. We use that threshold in constructing the final test contrastive conformal set.

**Remark 1.** *Our framework can be applied to any Euclidean semantic feature space, irrespective of the underlying pre-training paradigm. The designation “contrastive” does not require the backbone model itself to be trained via contrastive learning; rather, it describes our core objective of explicitly contrasting positive samples (for inclusion) against negative samples (for exclusion) to construct the covering sets.*

While the primary focus of this work is constructing contrastive conformal sets that guarantee positive sample inclusion while maximizing negative sample exclusion, we also explore their utility beyond strict uncertainty quantification. Specifically, we ask: *can contrastive conformal sets be employed off-the-shelf for downstream tasks without retraining?* To answer this, we evaluate our learned metric sets on a standard application in robust representation learning: out-of-distribution (OOD) detection.

**OOD Detection.** Metric sets trained on in-distribution (ID) data are specifically optimized to exclude ID negative samples. However, when these learned parameters are applied to OOD data, the separation between positive and negative samples deteriorates. This breakdown is reflected in a significantly reduced negative exclusion rate when evaluating OOD samples against the fixed, ID-calibrated threshold  $\hat{q}_\alpha$ . To exploit this phenomenon for OOD detection, we define an anomaly score as:

$$\text{OOD Score} = 1 - \text{negative exclusion rate.} \quad (23)$$

For ID data, the high negative exclusion rate enforced during training results in a low anomaly score. In contrast, the diminished exclusion rate for OOD data leads to a higher anomaly score, providing a robust and interpretable criterion for distinguishing OOD samples from ID samples.

## 5 EXPERIMENTS

We evaluate the proposed learned conformal sets on both simulated data and real-world image datasets. We assess performance based on three primary metrics: the coverage rate of positive samples, the exclusion rate of negative samples, and the log volume of the covering sets. As **no prior work has addressed this formulation**, we establish baselines using vanilla CP procedures utilizing the  $\ell_2$  norm and the Mahalanobis distance. To ensure a fair comparison and

avoid bias in the Mahalanobis baseline, we split the calibration data equally: one half is used to estimate the covariance matrix, while the remaining half is used to compute the conformity scores and empirical quantiles. We use the same conformal set to recalibrate the threshold for all methods post training.

**Simulated Data.** We first perform experiments on 3-dimensional simulated data drawn from various distributions. We compare our approach under three optimization objectives: minimizing only the log volume, maximizing only the approximate negative exclusion term, and optimizing the regularized objective introduced in (20). All simulated experiments are averaged over 40 random seeds.

**Image Classification.** For real-world evaluation, we utilize the CIFAR-100 dataset [Krizhevsky, 2009]. We employ a RepVGG-A2 architecture [Ding et al., 2021], pre-trained in a supervised manner with standard normalization techniques. We use the pre-trained weights obtained by Chen and made available here. We restrict our training to a random half of the CIFAR-100 training split. Image classification experiments are evaluated over 5 random seeds.

**OOD Detection.** Furthermore, we evaluate the models’ robustness in an OOD detection setting. We treat CIFAR-100 as the in-distribution (ID) dataset, and CIFAR-10 and SVHN as the OOD datasets. We compare against 9 commonly used OOD detection baselines: Maximum Softmax Probability (MSP) [Hendrycks and Gimpel, 2017], Energy (with temperature  $T = 1$ ) [Liu et al., 2020], K-Nearest neighbours (KNN) [Sun et al., 2022], Mahalanobis distance [Lee et al., 2018], COMBOOD [Rajasekaran et al., 2024], D-KNN [Peng et al., 2026], CIDER [Ming et al., 2023], and ViM [Wang et al., 2022]. More on the implementation details can be found in Appendix B.

**Evaluation metrics.** *Contrastive Conformal Sets:* We report (1) the coverage rate of positive samples, (2) the exclusion rate of negative samples, and (3) the LogVol of the produced metric set. *OOD:* We report (1) the false positive rate (FPR95) of OOD samples when the true positive rate of ID samples is at 95% and (2) the AUROC.

**Implementation Details.** We optimize the learnable metrics using Stochastic Gradient Descent (SGD). During training, we sample  $k = 20$  positive and negative instances without replacement for each anchor to ensure a robust gradient signal. When the InfoNCE loss is included, we jointly optimize the representations by alternating updates between the metric sets and the model’s penultimate layer weights at each epoch. For all methods, we perform model selection by evaluating the checkpoint that achieves the highest negative exclusion rate on the training split. The conformal misscoverage tolerance is strictly fixed at  $\alpha = 0.05$ . All results are reported as the mean  $\pm$  standard deviation across multiple

random seeds. Exhaustive details regarding hyperparameters, data splits, baseline configurations, and hardware are deferred to Appendix B.

## 6 RESULTS AND DISCUSSION

We evaluate our proposed methods on simulated 3D data, reporting positive coverage, negative exclusion, and log-volume (LogVol). We also assess downstream OOD detection using CIFAR-100 (ID) against CIFAR-10 (near-OOD) and SVHN (far-OOD). Extended metrics for CIFAR-100 and ImageNet-100, additional OOD evaluations (ImageNet-100 vs. NINCO and Textures), simulation implementation details, and a sensitivity analysis are deferred to the appendices (Appendices B, C and C.1). In all tables, the top three results are highlighted as **red**, **blue**, and **cyan**.

Table 1 presents the simulation results comparing the vanilla CP baselines with our proposed learned-metric methods. Note that the learned-metric conformal sets achieve substantially higher negative exclusion rates and lower log-volumes (LogVol). For example, the highest negative exclusion rate is achieved by the single-norm objective optimized for both volume and negative exclusion (Single (Vol)+Neg) at 49.0%. This is higher than the Mahalanobis Ellipsoid method’s exclusion rate by  $\approx 17\%$ , which is the strongest of the two vanilla CP baselines in this regard.

The average minimum LogVol, on the other hand, is achieved by the generalized multi-norm method optimized for both volume and negative exclusion (Generalized + Vol+Neg) at  $\approx -99.21$ . This is a significantly smaller volume compared to the Mahalanobis ellipsoid (LogVol  $\approx 6.51$ ), which yields the smallest volume among the vanilla baselines. In general, single-norm variants produce higher negative-exclusion rates due to more stable gradient convergence, while generalized multi-norm variants achieve lower LogVol, likely because the per-dimension exponents  $p_j$  can independently compress the bounding volume.

Table 1: Simulated 3D data clusters. Coverage, exclusion, and LogVol results for  $\alpha = 0.05$ .

Method	Coverage	Exclusion $\uparrow$	LogVol $\downarrow$
Conformal Ball ( $\ell_2$ )	95.0 $\pm$ 0.2%	18.8 $\pm$ 12.6%	7.36 $\pm$ 0.74
Mahalanobis Ellipsoid	95.0 $\pm$ 0.3%	32.4 $\pm$ 13.2%	6.51 $\pm$ 0.48
Single (Vol)	95.0 $\pm$ 0.2%	<b>42.9 <math>\pm</math> 11.5%</b>	6.25 $\pm$ 0.39
Generalized (Vol)	95.0 $\pm$ 0.2%	23.1 $\pm$ 12.2%	<b>-58.64 <math>\pm</math> 317.55</b>
Single (Neg)	95.0 $\pm$ 0.2%	<b>45.8 <math>\pm</math> 13.5%</b>	10.75 $\pm$ 3.22
Generalized (Neg)	95.0 $\pm$ 0.2%	39.6 $\pm$ 14.8%	<b>4.28 <math>\pm</math> 58.89</b>
Single (Neg, Vol)	95.0 $\pm$ 0.2%	<b>49.0 <math>\pm</math> 13.2%</b>	6.69 $\pm$ 0.61
Generalized (Neg, Vol)	95.0 $\pm$ 0.2%	34.8 $\pm$ 13.8%	<b>-99.21 <math>\pm</math> 445.68</b>

In Table 2, we compare the OOD detection results of our learned-metric contrastive conformal sets against eight baselines. To utilize our learned-metric sets for this task, we sample positive and negative instances for the given dataset, con-

struct the covering sets using the learned metrics, and compute an anomaly score defined as in (23). We noticed that subtracting also the positive exclusion rate yields slightly better results in this setting.

For CIFAR-100 (ID), this score is appropriately low since the exclusion of negatives is high. For CIFAR-10 and SVHN (OOD), the exclusion rate of negatives is conversely low (behaving similarly to the positive inclusion boundary), and hence the anomaly scores are very high. This separation in the derived metric space makes all learned-metric methods substantially outperform the baselines across both OOD datasets in AUROC and FPR95.

Table 2: OOD detection on CIFAR-100 (ID). Backbone: RepVGG-A2.

Method	SVHN		CIFAR10	
	AUROC $\uparrow$	FPR95 $\downarrow$	AUROC $\uparrow$	FPR95 $\downarrow$
MSP	78.3 $\pm$ 0.1	54.2 $\pm$ 0.3	79.8 $\pm$ 0.0	56.4 $\pm$ 0.1
Energy ( $T=1$ )	77.6 $\pm$ 0.2	54.0 $\pm$ 0.6	79.9 $\pm$ 0.0	56.4 $\pm$ 0.2
Mahalanobis	81.8 $\pm$ 0.0	54.4 $\pm$ 0.0	71.4 $\pm$ 0.0	72.3 $\pm$ 0.0
KNN ( $\ell_2$ )	32.1 $\pm$ 1.2	91.8 $\pm$ 0.5	19.7 $\pm$ 0.4	98.7 $\pm$ 0.1
COMBOOD	90.4 $\pm$ 0.0	41.5 $\pm$ 0.0	78.6 $\pm$ 0.0	60.8 $\pm$ 0.0
D-KNN	80.4 $\pm$ 0.0	55.9 $\pm$ 0.0	78.1 $\pm$ 0.0	62.6 $\pm$ 0.0
CIDER	77.5 $\pm$ 0.3	54.6 $\pm$ 0.6	77.8 $\pm$ 0.1	59.5 $\pm$ 0.3
ViM	83.4 $\pm$ 0.0	50.5 $\pm$ 0.0	72.9 $\pm$ 0.0	65.2 $\pm$ 0.0
Generalized (Neg)	98.0 $\pm$ 0.2	8.3 $\pm$ 0.2	88.2 $\pm$ 1.0	63.8 $\pm$ 6.9
Single (Neg)	98.2 $\pm$ 0.4	<b>8.1 <math>\pm</math> 3.4</b>	91.8 $\pm$ 0.5	49.9 $\pm$ 3.6
Generalized (Vol)	<b>99.2 <math>\pm</math> 0.2</b>	<b>1.7 <math>\pm</math> 1.5</b>	95.1 $\pm$ 0.6	35.5 $\pm$ 5.4
Single (Vol)	96.2 $\pm$ 2.0	23.1 $\pm$ 13.8	<b>96.2 <math>\pm</math> 0.2</b>	<b>22.2 <math>\pm</math> 2.3</b>
Single (Neg, Vol)	96.8 $\pm$ 1.6	20.2 $\pm$ 12.9	<b>95.7 <math>\pm</math> 1.4</b>	<b>28.9 <math>\pm</math> 12.8</b>
Generalized (Neg, Vol)	<b>99.2 <math>\pm</math> 0.2</b>	<b>1.7 <math>\pm</math> 0.9</b>	95.4 $\pm$ 0.3	34.5 $\pm$ 2.3
Single (Neg, Vol, InfoNCE)	<b>98.5 <math>\pm</math> 0.9</b>	8.2 $\pm$ 6.6	95.2 $\pm$ 1.6	31.3 $\pm$ 11.6
Generalized (Neg, Vol, InfoNCE)	97.6 $\pm$ 0.8	15.6 $\pm$ 7.0	<b>96.3 <math>\pm</math> 0.8</b>	<b>26.0 <math>\pm</math> 7.7</b>

## 7 CONCLUSION

This work extends the principles of CP to semantic feature spaces by introducing contrastive conformal sets. These sets are designed as minimum-volume, generalized multi-norm regions that guarantee the inclusion of positive samples with a user-specified probability, while simultaneously maximizing the exclusion of negative samples. The proposed framework is broadly applicable to any Euclidean semantic feature space, including those generated by pretrained contrastive models. These certified covering sets provide a principled mechanism for quantifying the uncertainty of semantic representations (e.g., self-supervised embeddings) and enable robust OOD detection.

Future work will explore leveraging the geometric properties of these certified sets for downstream tasks directly within their boundaries. Additionally, the current formulation is limited to Euclidean metrics and does not address Riemannian manifold geometries or other non-Euclidean spaces. Extending the framework to accommodate such complex geometries represents a promising direction for further research.

## References

- Anastasios N. Angelopoulos and Stephen Bates. A gentle introduction to conformal prediction and distribution-free uncertainty quantification. *arXiv preprint arXiv:2107.07511*, 2022.
- Anastasios N. Angelopoulos, Rina Foygel Barber, and Stephen Bates. *Theoretical Foundations of Conformal Prediction*. 2025. URL <https://arxiv.org/abs/2411.11824>. Forthcoming, Cambridge University Press. arXiv:2411.11824v3.
- Shervin Ardeshtir and Navid Azizan. Embedding reliability: On the predictability of downstream performance. In *ML Safety Workshop, 36th Conference on Neural Information Processing Systems (NeurIPS 2022)*, 2022. URL <https://openreview.net/forum?id=TedqYedIERd>. Workshop paper.
- Bernhard E. Boser, Isabelle M. Guyon, and Vladimir N. Vapnik. A training algorithm for optimal margin classifiers. In *Proceedings of the Fifth Annual Workshop on Computational Learning Theory, COLT '92*, pages 144–152, Pittsburgh, PA, USA, July 1992. ACM Press. doi: 10.1145/130385.130401. URL <https://doi.org/10.1145/130385.130401>.
- Sacha Braun, Liviu Aolaritei, Michael I. Jordan, and Francis Bach. Minimum volume conformal sets for multivariate regression. *arXiv preprint arXiv:2503.19068*, 2025. doi: 10.48550/arXiv.2503.19068.
- Ting Chen, Simon Kornblith, Mohammad Norouzi, and Geoffrey Hinton. A simple framework for contrastive learning of visual representations. In *Proceedings of the 37th International Conference on Machine Learning*, volume 119 of *Proceedings of Machine Learning Research*, pages 1597–1607. PMLR, 13–18 Jul 2020. URL <http://proceedings.mlr.press/v119/chen20j.html>.
- Yaofu Chen. Pytorch cifar models. <https://github.com/chenafo/pytorch-cifar-models>. Accessed: 2026-01-15.
- Ching-Yao Chuang, Joshua Robinson, Yen-Chen Lin, Antonio Torralba, and Stefanie Jegelka. Debaised contrastive learning. In *Advances in Neural Information Processing Systems (NeurIPS)*, volume 33, 2020.
- Xiaohan Ding, Xiangyu Zhang, Ningning Ma, Jungong Han, Guiguang Ding, and Jian Sun. Repvgg: Making vgg-style convnets great again. In *Proceedings of the IEEE/CVF Conference on Computer Vision and Pattern Recognition (CVPR)*, pages 13733–13742, June 2021.
- Tai Dinh, Wong Hauchia, Daniil Lisik, Michal Koren, Dat Tran, Philip S. Yu, and Joaquín Torres-Sospedra. Data clustering: An essential technique in data science. *arXiv preprint arXiv:2412.18760*, 2025.
- Jacopo Diquigiovanni, Matteo Fontana, and Simone Vantini. Conformal prediction bands for multivariate functional data. *Journal of Multivariate Analysis*, 189:104879, 2022. doi: 10.1016/j.jmva.2021.104879.
- Rina Foygel Barber, Emmanuel J. Candès, Aaditya Ramdas, and Ryan J. Tibshirani. Conformal prediction beyond exchangeability. *The Annals of Statistics*, 51(2):816–845, 2023. doi: 10.1214/23-AOS2276. URL <https://projecteuclid.org/journals/annals-of-statistics/volume-51/issue-2/Conformal-prediction-beyond-exchangeability/10.1214/23-AOS2276.full>.
- Dan Hendrycks and Kevin Gimpel. A baseline for detecting misclassified and out-of-distribution examples in neural networks. In *International Conference on Learning Representations*, 2017.
- Edwin Hewitt and Leonard J. Savage. Symmetric measures on cartesian products. *Transactions of the American Mathematical Society*, 80(2):470–501, 1955. ISSN 00029947, 10886850. URL <http://www.jstor.org/stable/1992999>.
- Chancellor Johnstone and Bruce Cox. Conformal uncertainty sets for robust optimization. In Lars Carlsson, Zhiyuan Luo, Giovanni Cherubin, and Khuong An Nguyen, editors, *Proceedings of the Tenth Symposium on Conformal and Probabilistic Prediction and Applications*, volume 152 of *Proceedings of Machine Learning Research*, pages 72–90. PMLR, 08–10 Sep 2021.
- Prannay Khosla, Piotr Teterwak, Chen Wang, Aaron Sarna, Yonglong Tian, Phillip Isola, Aaron Maschinot, Ce Liu, and Dilip Krishnan. Supervised contrastive learning. In *Advances in Neural Information Processing Systems (NeurIPS)*, volume 33, 2020.
- Michal Klein, Louis Bethune, Eugene Ndiaye, and Marco Cuturi. Multivariate conformal prediction using optimal transport. *arXiv preprint arXiv:2502.03609*, February 2025. URL <https://arxiv.org/abs/2502.03609>.
- Alex Krizhevsky. Learning multiple layers of features from tiny images. Technical report, 2009.
- Kimin Lee, Kibok Lee, Honglak Lee, and Jinwoo Shin. A simple unified framework for detecting out-of-distribution samples and adversarial attacks. In *Advances in Neural Information Processing Systems*, volume 31, 2018.

- Jing Lei, Alessandro Rinaldo, and Larry Wasserman. A conformal prediction approach to explore functional data. *Annals of Mathematics and Artificial Intelligence*, 74(1): 29–43, 2015. doi: 10.1007/s10472-013-9366-6.
- Hao Liu and Pieter Abbeel. Hybrid discriminative-generative training via contrastive learning. *arXiv preprint arXiv:2007.09070*, 2020.
- Weitang Liu, Xiaoyun Wang, John Owens, and Yixuan Li. Energy-based out-of-distribution detection. In *Advances in Neural Information Processing Systems*, volume 33, pages 21464–21475, 2020.
- Yibing Liu, Chris XING TIAN, Haoliang Li, Lei Ma, and Shiqi Wang. Neuron activation coverage: Rethinking out-of-distribution detection and generalization. In *The Twelfth International Conference on Learning Representations*, 2024. URL <https://openreview.net/forum?id=SNGXbZtK6Q>.
- Leland McInnes, John Healy, Nathaniel Saul, and Lukas Großberger. Umap: Uniform manifold approximation and projection. *Journal of Open Source Software*, 3(29): 861, 2018. doi: 10.21105/joss.00861. URL <https://doi.org/10.21105/joss.00861>.
- Soundouss Messoudi, Sébastien Destercke, and Sylvain Rousseau. Conformal multi-target regression using neural networks. In Alexander Gammerman, Vladimir Vovk, Zhiyuan Luo, Evgueni Smirnov, and Giovanni Cherubin, editors, *Proceedings of the Ninth Symposium on Conformal and Probabilistic Prediction and Applications*, volume 128 of *Proceedings of Machine Learning Research*, pages 65–83. PMLR, 09–11 Sep 2020. URL <https://proceedings.mlr.press/v128/messoudi20a.html>.
- Yifei Ming, Yiyu Sun, Ousmane Dia, and Yixuan Li. How to exploit hyperspherical embeddings for out-of-distribution detection? In *The Eleventh International Conference on Learning Representations*, 2023. URL <https://openreview.net/forum?id=aEFaE0W5pAd>.
- Seong Joon Oh, Kevin Murphy, Jiyan Pan, Joseph Roth, Florian Schroff, and Andrew Gallagher. Modeling uncertainty with hedged instance embedding. In *International Conference on Learning Representations (ICLR)*, 2019.
- Ningkang Peng, Xiaoqian Peng, Yuhao Zhang, Qianfeng Yu, Feng Xing, Peirong Ma, Xichen Yang, Yi Chen, Tingyu Lu, and Yanhui Gu. Breaking semantic hegemony: Decoupling principal and residual subspaces for generalized ood detection, 2026. URL <https://arxiv.org/abs/2602.05360>.
- Victor Quach, Adam Fisch, Tal Schuster, Adam Yala, Jae Ho Sohn, Tommi S. Jaakkola, and Regina Barzilay. Conformal language modeling. In *International Conference on Learning Representations*, 2024. URL <https://openreview.net/forum?id=pzUhfQ74c5>.
- Magesh Rajasekaran, Md Saiful Islam Sajol, Frej Berglind, Supratik Mukhopadhyay, and Kamalika Das. *COMBOOD: A Semiparametric Approach for Detecting Out-of-distribution Data for Image Classification*, pages 643–651. 2024. doi: 10.1137/1.9781611978032.74. URL <https://epubs.siam.org/doi/abs/10.1137/1.9781611978032.74>.
- Nikunj Saunshi, Orestis Plevrakis, Sanjeev Arora, Mikhail Khodak, and Hrishikesh Khandeparkar. A theoretical analysis of contrastive unsupervised representation learning. In *Proceedings of the 36th International Conference on Machine Learning (ICML)*, volume 97 of *Proceedings of Machine Learning Research*, pages 5628–5637. PMLR, 2019.
- Florian Schroff, Dmitry Kalenichenko, and James Philbin. Facenet: A unified embedding for face recognition and clustering. In *Proceedings of the IEEE Conference on Computer Vision and Pattern Recognition*, CVPR, pages 815–823. IEEE, 2015. URL [https://www.cv-foundation.org/openaccess/content\\_cvpr\\_2015/papers/Schroff\\_FaceNet\\_A\\_Unified\\_2015\\_CVPR\\_paper.pdf](https://www.cv-foundation.org/openaccess/content_cvpr_2015/papers/Schroff_FaceNet_A_Unified_2015_CVPR_paper.pdf).
- Glenn Shafer and Vladimir Vovk. *Conformal Prediction for Reliable Machine Learning: Theory, Adaptations, and Applications*. Elsevier, 2008. ISBN 9780123985378.
- Ambesh Shekhar. Imagenet100: A sample of imagenet classes. Kaggle Dataset, August 2021. URL <https://www.kaggle.com/datasets/ambityga/imagenet100>.
- Liangliang Shi, Gu Zhang, Haoyu Zhen, Jintao Fan, and Junchi Yan. Understanding and generalizing contrastive learning from the inverse optimal transport perspective. In *Proceedings of the 40th International Conference on Machine Learning*, volume 202 of *Proceedings of Machine Learning Research*. PMLR, 2023.
- Yiyu Sun, Yifei Ming, Xiaojin Zhu, and Yixuan Li. Out-of-distribution detection with deep nearest neighbors. In *International Conference on Machine Learning*, pages 20827–20840. PMLR, 2022.
- Jihoon Tack, Sangwoo Mo, Jongheon Jeong, and Jinwoo Shin. CSI: Novelty detection via contrastive learning on distributionally shifted instances. In *Advances in Neural Information Processing Systems (NeurIPS)*, volume 33, 2020.

Jiaye Teng, Chuan Wen, Dinghuai Zhang, Yoshua Bengio, Yang Gao, and Yang Yuan. Predictive inference with feature conformal prediction. In *The Eleventh International Conference on Learning Representations*, 2023. URL <https://openreview.net/forum?id=0uRmlYmFTu>.

Aaron van den Oord, Yazhe Li, and Oriol Vinyals. Representation learning with contrastive predictive coding. *arXiv preprint arXiv:1807.03748*, 2018.

Vladimir Vovk, Alex Gammerman, and Glenn Shafer. *Algorithmic Learning in a Random World*. Springer, New York, 2005.

Haoqi Wang, Zhizhong Li, Litong Feng, and Wayne Zhang. ViM: Out-Of-Distribution with Virtual-logit Matching. In *2022 IEEE/CVF Conference on Computer Vision and Pattern Recognition (CVPR)*, pages 4911–4920, Los Alamitos, CA, USA, June 2022. IEEE Computer Society. doi: 10.1109/CVPR52688.2022.00487. URL <https://doi.ieeecomputersociety.org/10.1109/CVPR52688.2022.00487>.

Xianfu Wang. Volumes of generalized unit balls. *Mathematics Magazine*, 78(5):390–395, 2005. ISSN 0025570X, 19300980. URL <http://www.jstor.org/stable/30044198>.

Yandong Wen, Kaipeng Zhang, Zhifeng Li, and Yu Qiao. A discriminative feature learning approach for deep face recognition. In Bastian Leibe, Jiri Matas, Nicu Sebe, and Max Welling, editors, *Computer Vision – ECCV 2016*, pages 499–515, Cham, 2016. Springer International Publishing. ISBN 978-3-319-46478-7.

Jim Winkens, Rudy Bunel, Abhijit Guha Roy, Robert Stanforth, Vivek Natarajan, Joseph R. Ledsam, Patricia MacWilliams, Pushmeet Kohli, Alan Karthikesalingam, Simon Kohl, Taylan Cemgil, S. M. Ali Eslami, and Olaf Ronneberger. Contrastive training for improved out-of-distribution detection. *arXiv preprint arXiv:2007.05566*, 2020.

Mike Wu and Noah Goodman. A simple framework for uncertainty in contrastive learning. *arXiv preprint arXiv:2010.02038*, 2020.

Yanqiao Zhu, Yichen Xu, Feng Yu, Qiang Liu, Shu Wu, and Liang Wang. Deep graph contrastive representation learning. *arXiv preprint arXiv:2006.04131*, June 2020. URL <https://arxiv.org/abs/2006.04131>.

---

# Contrastive Conformal Sets (Supplementary Material)

---

Yahya Alkhatib<sup>1</sup>

Wee Peng Tay<sup>1</sup>

<sup>1</sup>School of Electrical and Electronic Engineering, Nanyang Technological University, Singapore

## A PROOF OF THEORETICAL RESULTS AND COMPLEXITY ANALYSIS

This section presents proofs of the theoretical results established in the main paper, alongside a comprehensive computational complexity analysis of the proposed methodology.

### A.1 PROOF OF Corollary 1

Let  $\mathcal{E}_{\text{pos}} \triangleq \{Z_{\text{pos}} \in \mathcal{N}(Z)\}$ ,  $\mathcal{E}_{\text{neg}} \triangleq \{Z_{\text{neg}} \notin \mathcal{N}(Z)\}$ , and define the event that the positive sample shares the anchor's class as  $E \triangleq \{Y_{\text{pos}} = Y\}$ .

From (6b), we have  $\mathbb{P}(\mathcal{E}_{\text{pos}}^c) \leq \alpha$ . Applying the Law of Total Probability, we can expand this as:

$$\begin{aligned} \alpha &\geq \mathbb{P}(\mathcal{E}_{\text{pos}}^c) = \mathbb{P}(E) \mathbb{P}(\mathcal{E}_{\text{pos}}^c | E) + \mathbb{P}(E^c) \mathbb{P}(\mathcal{E}_{\text{pos}}^c | E^c) \\ &\geq \mathbb{P}(E) \mathbb{P}(\mathcal{E}_{\text{pos}}^c | E). \end{aligned} \quad (24)$$

Rearranging the terms to isolate the conditional probability yields the oracle positive inclusion bound:

$$\mathbb{P}(\mathcal{E}_{\text{pos}} | E) \geq 1 - \frac{\alpha}{\mathbb{P}(E)} = 1 - \frac{\alpha}{\mathbb{P}(Y_{\text{pos}} = Y)}. \quad (25)$$

Similarly, for the negative exclusion rate, let  $E' \triangleq \{Y_{\text{neg}} \neq Y\}$ . Given that the exclusion probability satisfies  $\mathbb{P}(\mathcal{E}_{\text{neg}}^c) \leq \beta$ , an analogous expansion gives:

$$\beta \geq \mathbb{P}(\mathcal{E}_{\text{neg}}^c) \geq \mathbb{P}(E') \mathbb{P}(\mathcal{E}_{\text{neg}}^c | E'), \quad (26)$$

which directly implies the oracle negative exclusion bound:

$$\mathbb{P}(\mathcal{E}_{\text{neg}} | E') \geq 1 - \frac{\beta}{\mathbb{P}(E')} = 1 - \frac{\beta}{\mathbb{P}(Y_{\text{neg}} \neq Y)}. \quad (27)$$

This completes the proof.

### A.2 PROOF OF Lemma 1

Let  $V^j = (Z^j, Z_{\text{pos}}^j)$  for  $j = 1, \dots, n_{\text{cal}}$  denote the pairs of embeddings corresponding to the calibration anchors and their associated positive samples. Similarly, let  $V^{n_{\text{cal}}+1} = (Z, Z_{\text{pos}})$  denote the pair of embeddings for the test anchor and its associated positive sample. It suffices to show that the set of pairs  $\{V^1, \dots, V^{n_{\text{cal}}+1}\}$  is exchangeable. The result then follows from the standard conformal prediction coverage guarantee [Angelopoulos et al., 2025].

Denote  $X^{n_{\text{cal}}+1} = X$ . From de Finetti's theorem [Hewitt and Savage, 1955], since  $(X^1, \dots, X^{n_{\text{cal}}+1})$  are exchangeable, there exists a latent variable  $W$  such that the sequence is conditionally independent and identically distributed (i.i.d.) given  $W$ . We therefore have:

$$\begin{aligned}
& p_{V^1, \dots, V^{n_{\text{cal}}+1} | W}(v^1, \dots, v^{n_{\text{cal}}+1} | w) \\
&= \int p(v^1, \dots, v^{n_{\text{cal}}+1} | w, x^1, \dots, x^{n_{\text{cal}}+1}) p(x^1, \dots, x^{n_{\text{cal}}+1} | w) dx^1 \dots dx^{n_{\text{cal}}+1} \\
&= \int \prod_{j=1}^{n_{\text{cal}}+1} p(v^j | w, x^j) \prod_{j=1}^{n_{\text{cal}}+1} p(x^j | w) dx^1 \dots dx^{n_{\text{cal}}+1} \\
&= \int \prod_{j=1}^{n_{\text{cal}}+1} p(v^j, x^j | w) dx^1 \dots dx^{n_{\text{cal}}+1} \\
&= \prod_{j=1}^{n_{\text{cal}}+1} \int p(v^j, x^j | w) dx^j \\
&= \prod_{j=1}^{n_{\text{cal}}+1} p(v^j | w),
\end{aligned}$$

where the second equality follows from the fact that given  $W$ , the anchors  $(X^1, \dots, X^{n_{\text{cal}}+1})$  are independent and the generation mechanism of  $X_{\text{pos}}^j$  depends only on  $X^j$ . Therefore, the sequence of pairs  $(V^1, \dots, V^{n_{\text{cal}}+1})$  is conditionally i.i.d. given  $W$ . This implies that the sequence is exchangeable, which completes the proof.

### A.3 PROOF OF Proposition 1

Recall that  $Z_{\text{pos}} = \theta(X_{\text{pos}})$  and  $Z_{\text{neg}} = \theta(X_{\text{neg}})$ , where  $X_{\text{pos}}$  and  $X_{\text{neg}}$  are the positive and negative samples associated with  $X$  under the mechanisms  $p_{\text{pos}}(\cdot | X)$  and  $p_{\text{neg}}(\cdot | X)$ , respectively. For  $t \in T$ , define

$$p_+(t) \triangleq \mathbb{P}(Z_{\text{pos}} \in \mathcal{B}_t), \quad p_-(t) \triangleq \mathbb{P}(Z_{\text{neg}} \in \mathcal{B}_t), \quad q_-(t) \triangleq \mathbb{P}(Z_{\text{neg}} \notin \mathcal{B}_t) = 1 - p_-(t).$$

By the nesting assumption, if  $t_1 \leq t_2$  then

$$\mathcal{B}_{t_1} \subseteq \mathcal{B}_{t_2},$$

hence

$$\{Z_{\text{pos}} \in \mathcal{B}_{t_1}\} \subseteq \{Z_{\text{pos}} \in \mathcal{B}_{t_2}\}, \quad \{Z_{\text{neg}} \in \mathcal{B}_{t_1}\} \subseteq \{Z_{\text{neg}} \in \mathcal{B}_{t_2}\}.$$

By monotonicity of probability,

$$p_+(t_1) \leq p_+(t_2) \quad \text{and} \quad p_-(t_1) \leq p_-(t_2),$$

so  $p_+$  and  $p_-$  are non-decreasing in  $t$ . Consequently,

$$q_-(t) = 1 - p_-(t)$$

is non-increasing in  $t$ . Next, consider the set of indices for which the positive inclusion requirement is satisfied:

$$T_\alpha \triangleq \{t \in T : p_+(t) \geq 1 - \alpha\}.$$

Any  $t \in T_\alpha$  corresponds to a set  $\mathcal{B}_t$  satisfying (6b). Since  $p_+$  is non-decreasing,  $T_\alpha$  is either empty or an upper set in  $T$  (if  $t_0 \in T_\alpha$  and  $t \geq t_0$ , then  $t \in T_\alpha$ ). Assume  $T_\alpha \neq \emptyset$  and let  $t^*$  be any solution of (18). In particular,  $t^* \in T_\alpha$ , so  $\mathcal{B}_\alpha^* = \mathcal{B}_{t^*}$  satisfies the positive inclusion requirement (6b). Now take any  $t \in T_\alpha$ . By the definition of  $t^*$  as a minimizer of  $\text{Vol}(\mathcal{B}_t)$  over  $T_\alpha$ , and by the monotonicity of  $\text{Vol}(\mathcal{B}_t)$  in  $t$ , we must have  $t \geq t^*$ . Since  $q_-(t)$  is non-increasing in  $t$ , it follows that

$$q_-(t) \leq q_-(t^*) \quad \text{for all } t \in T_\alpha.$$

Equivalently,

$$\mathbb{P}(Z_{\text{neg}} \notin \mathcal{B}_t) \leq \mathbb{P}(Z_{\text{neg}} \notin \mathcal{B}_{t^*}) \quad \forall t \in T_\alpha.$$

Thus, among all sets  $\mathcal{B}_t$  that satisfy the positive inclusion constraint,  $\mathcal{B}_\alpha^*$  attains the largest negative exclusion probability (6a). Finally, by construction in (18),  $\mathcal{B}_\alpha^*$  also minimizes  $\text{Vol}(\mathcal{B}_t)$  over  $T_\alpha$ , i.e. it has minimum volume among all sets in the family  $\{\mathcal{B}_t : t \in T\}$  that satisfy (6b). This proves the claim.

## A.4 COMPLEXITY ANALYSIS

In this analysis, we assume semantic feature vectors of dimensionality  $d$ .

**Vanilla CP Complexity.** Assume a calibration set  $\mathcal{D}_{\text{cal}}$  of size  $n_{\text{cal}} \gg d$ . For the vanilla CP baselines, we compute the positive distances for all calibration points and extract the empirical  $\lceil (1 - \alpha)(n_{\text{cal}} + 1) \rceil / n_{\text{cal}}$  quantile. In the  $\ell_p$  norm case, computing the  $d$ -dimensional differences takes  $\mathcal{O}(n_{\text{cal}}d)$ , and sorting them to find the quantile takes  $\mathcal{O}(n_{\text{cal}} \log n_{\text{cal}})$ . Thus, the overall complexity is  $\mathcal{O}(n_{\text{cal}}(d + \log n_{\text{cal}}))$ . For the Mahalanobis distance baseline, we must first estimate the  $d \times d$  covariance matrix, which requires  $\mathcal{O}(n_{\text{cal}}d^2)$  operations, and then invert it, taking  $\mathcal{O}(d^3)$  operations. Computing the distances for the calibration points then takes an additional  $\mathcal{O}(n_{\text{cal}}d^2)$ . Since  $n_{\text{cal}} \gg d$ , the covariance estimation and distance computations dominate the matrix inversion, resulting in a total complexity of  $\mathcal{O}(n_{\text{cal}}d^2 + n_{\text{cal}} \log n_{\text{cal}})$ .

**Learnable-Metric Conformal Sets Complexity.** Assume a training set  $\mathcal{D}_{\text{train}}$  of size  $n_{\text{train}} \gg d$  and a training duration of  $k$  epochs. For the single-norm sets, computing the distances requires a matrix-vector multiplication for each sample, incurring a cost of  $\mathcal{O}(n_{\text{train}}d^2)$  per epoch. Additionally, calculating the empirical  $\lceil (1 - \alpha)(n + 1) \rceil / n$  quantile of the positive distances requires sorting at each epoch, which adds  $\mathcal{O}(n_{\text{train}} \log n_{\text{train}})$ . Thus, over  $k$  epochs, the total training complexity is  $\mathcal{O}(kn_{\text{train}}(d^2 + \log n_{\text{train}}))$ . Because the squared dimensionality  $d^2$  is typically large in deep learning semantic spaces, the matrix multiplication term  $\mathcal{O}(kn_{\text{train}}d^2)$  dominates the sorting term. Conversely, the generalized multi-norm sets only require element-wise scaling and power operations, reducing the distance computation per epoch to  $\mathcal{O}(n_{\text{train}}d)$ . The overall training complexity for the generalized multi-norm is therefore bounded by  $\mathcal{O}(kn_{\text{train}}(d + \log n_{\text{train}}))$ , making it significantly more computationally efficient than both the single-norm approach and the vanilla Mahalanobis baseline.

## B REPRODUCIBILITY DETAILS

**3D Simulation Setup (Mixed Distribution).** To evaluate the learned metrics on complex, non-spherical geometries, we simulate a 3D dataset ( $d = 3$ ) comprising 5 distinct classes, each containing 5,000 points. The cluster centers are uniformly distributed along a circle of radius 2.5 with a slight sinusoidal elevation in the  $z$ -axis. To create the “mixed” geometry, the first two classes are generated as anisotropic Gaussians by stretching a random covariance matrix along a randomly selected axis by a factor of  $U(3, 5)$ . The remaining three classes are generated as “banana” (crescent) distributions by sampling points along 3D arcs (base radius 1.5), applying random orthogonal rotations, and injecting isotropic Gaussian noise ( $\sigma = 1.0$ ). See Fig. 2.

For the experimental pipeline, we bypass the neural encoder and optimize the metric parameters directly on the 3D coordinates. The dataset is partitioned into 60% for training and 40% for conformal calibration and testing (split equally). During training, we sample  $k = 200$  positive and negative instances per anchor. The metric parameters are optimized for 30 epochs using SGD with a learning rate of 0.01, a batch size of 256, and gradient clipping at 1.0. For methods incorporating volume regularization, the balancing weight is set to  $\lambda = 0.05$ .

**Datasets and Pretrained Models.** We conduct experiments on CIFAR-100 [Krizhevsky, 2009], accessed directly via `torchvision`, and ImageNet-100 [Shekhar, 2021], a 100-class subset of ImageNet available via Kaggle. CIFAR-100 experiments are averaged over 5 random seeds, while ImageNet-100 experiments are averaged over 3 random seeds. For our backbones, we utilize a ResNet-18 model pretrained on ImageNet-1K (loaded via `torchvision`) and a RepVGG-a2 model, with pretrained weights downloaded from this repository.

**Data Splitting and Calibration.** To learn the conformal metric sets, we utilize a random 50% subset of the CIFAR-100 training split and a 10% subset of the ImageNet-100 training split. For the conformal calibration phase (i.e., determining the quantile threshold  $\hat{q}_\alpha$ ), we use 50% of the validation/test splits, reserving the remaining 50% strictly for final evaluation. For all variants of our method, we sample  $k = 20$  positive and  $k = 20$  negative instances from the same class and different classes, respectively, adhering to the supervised setting. The conformal miscoverage tolerance is fixed at  $\alpha = 0.05$  across all experiments, following standard practice.

**Optimization and Hyperparameters.** We train the metric sets using Stochastic Gradient Descent (SGD) with a learning rate of 0.1, a momentum of 0.9, and a weight decay of  $5 \times 10^{-4}$ , annealed using a `CosineAnnealingLR` scheduler. The batch size is set to 256. To stabilize training, gradients are clipped at a maximum norm of 1.0, and the sigmoid temperature for the negative exclusion loss is fixed at 7.0. When the InfoNCE loss is excluded, the metric sets are optimized for 30

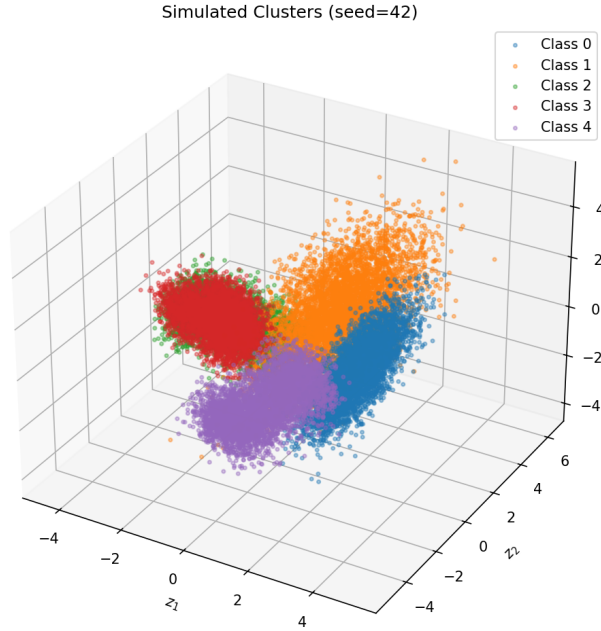


Figure 2: 3D Simulation Mixed Data Distribution

epochs. When the InfoNCE loss is included, we train for a total of 50 epochs, alternating between updating the metric sets and the model weights. To preserve the pretrained representations, we restrict the model updates strictly to the penultimate layer’s weights. For methods incorporating volume regularization (Neg+Vol), the balancing weight is set to  $\lambda = 0.05$  while the constant before the negative objective remains 1.0. The InfoNCE weight is  $\lambda_{\text{InfoNCE}} = 1.0$ , with the InfoNCE temperature fixed at  $\tau = 0.1$ . Regardless of the specific optimization objective, we always checkpoint and evaluate the model that achieves the highest negative exclusion rate on the training split.

**Baseline Configurations.** For the out-of-distribution (OOD) detection baselines, the Energy score temperature is fixed at  $T = 1.0$ . For the remaining baselines, we follow the hyperparameter configurations recommended in their respective original papers:

- **COMBOOD:**  $k = 50, C = 1.0$ . We extract the maximum activations exclusively from the ReLU layers, as these constitute the vast majority of activations in both ResNet-18 and RepVGG-a2 architectures.
- **D-KNN:**  $k = 50, d = 0.95, \alpha = 0.5$ .
- **CIDER:** Projection dimension = 128, epochs = 100, learning rate = 0.5,  $\tau = 0.1, \lambda_c = 2.0, \alpha = 0.999$ . To ensure a fair comparison with our method, we freeze the backbone and only train the projection head for fair comparison as the other methods do not train the backbone.
- **NAC:** [Liu et al., 2024]  $\alpha = 100.0, r = 1.0$ , number of bins = 1000. We extract the maximum activations exclusively from the fully connected layer, which yielded the best empirical results during our testing compared to other layer combinations.

**Hardware Configuration.** Experiments were distributed across four NVIDIA RTX A5000 GPUs, with the exception of the OOD evaluations, which utilized three of these GPUs.

**Code Availability.** To ensure full reproducibility, the complete source code, including data preprocessing scripts, training routines, and evaluation protocols, will be made publicly available upon the acceptance of this manuscript.

## C MORE RESULTS

Tables 3 and 4 report coverage, exclusion, and LogVol results on the image benchmarking datasets CIFAR-100 and ImageNet-100 using the pretrained models RepVGG-A2 and ResNet18, respectively. We can see a somewhat similar trend to the simulation data. The two vanilla CP baselines are outperformed in terms of negative exclusion rates and LogVol by several learned-metric methods. This suggests that by optimizing directly for the negative exclusion rate or the volume of the conformal covering sets, one can achieve a superior balance of the two objectives. Note that optimizing the generalized multi-norm metric yields, relatively, smaller LogVol for the resulting sets. As introduced in our methodology, this volume reduction is likely driven by the optimizer increasing the dimension-wise exponents  $p_j$ . As  $p_j \gg 2$ , the generalized multi-norm sets transition from smooth, spherical boundaries to sharper, hyper-rectangular geometries. Combined with dimension-specific scaling, this allows the sets to tightly pack around the data distribution, discarding the wasted empty volume typical of smooth ellipsoids.

Table 5 reports the OOD detection results on ImageNet-100 (ID) against NINCO (near-OOD) and Textures (far-OOD), averaged over 3 random seeds. These results demonstrate that the learned contrastive conformal sets can be effectively utilized for anomaly detection even on highly complex image distributions. Furthermore, variants optimized with the joint Neg+InfoNCE objective exhibit substantial improvements in differentiating ID from OOD samples, achieving near-perfect detection on the far-OOD benchmark. Notably, these same variants also yield the highest negative exclusion rates in Table 4, confirming a strong correlation between learning tightly bounded, high-exclusion conformal sets and achieving robust downstream OOD detection. Table 6 reports the OOD detection results on SLT10 (ID) against CIFAR10 (near-OOD), CIFAR100 (near-OOD) and SVHN (far-OOD), averaged over 3 random seeds, and the positive/negative generation is by augmentation. The backbone ResNet18 model is trained using SimCLR contrastive learning without label information.

Table 3: CIFAR-100, model=RepVGG-A2,  $k = 20$ ,  $\alpha = 0.05$ ,  $n_{\text{test}} = 5000$ , seeds=5.

Method	Coverage	Exclusion $\uparrow$	LogVol $\downarrow$
Conformal Ball ( $\ell_2$ )	95.0 $\pm$ 0.0%	67.8 $\pm$ 0.1%	519.3 $\pm$ 1.6
Mahalanobis Ellipsoid	95.0 $\pm$ 0.1%	10.8 $\pm$ 0.1%	-2233.1 $\pm$ 1.6
Single (Vol)	94.8 $\pm$ 0.0%	56.8 $\pm$ 0.8%	-1127.0 $\pm$ 201.0
Generalized (Vol)	94.8 $\pm$ 0.1%	66.5 $\pm$ 0.9%	-429.8 $\pm$ 4.7
Single (Neg)	94.9 $\pm$ 0.1%	<b>77.6 <math>\pm</math> 0.4%</b>	3044.4 $\pm$ 38.7
Generalized (Neg)	94.9 $\pm$ 0.1%	74.8 $\pm$ 0.2%	149.4 $\pm$ 100.1
Single (Vol, InfoNCE)	94.9 $\pm$ 0.1%	56.4 $\pm$ 0.9%	<b>-2236.9 <math>\pm</math> 405.3</b>
Generalized (Vol, InfoNCE)	94.9 $\pm$ 0.0%	56.7 $\pm$ 0.5%	<b>-4063.5 <math>\pm</math> 240.0</b>
Single (Neg, InfoNCE)	94.9 $\pm$ 0.0%	<b>76.8 <math>\pm</math> 0.5%</b>	1977.7 $\pm$ 55.2
Generalized (Neg, InfoNCE)	94.8 $\pm$ 0.1%	<b>76.2 <math>\pm</math> 0.3%</b>	-508.0 $\pm$ 143.3
Single (Neg, Vol)	95.0 $\pm$ 0.1%	57.6 $\pm$ 0.5%	-1100.2 $\pm$ 276.5
Generalized (Neg, Vol)	94.8 $\pm$ 0.1%	66.4 $\pm$ 0.7%	-422.9 $\pm$ 8.7
Single (Neg, Vol, InfoNCE)	94.9 $\pm$ 0.0%	58.9 $\pm$ 0.3%	-1939.1 $\pm$ 127.2
Generalized (Neg, Vol, InfoNCE)	94.8 $\pm$ 0.2%	59.7 $\pm$ 1.4%	<b>-3850.9 <math>\pm</math> 567.4</b>

### C.1 SENSITIVITY ANALYSIS

We present a sensitivity analysis for a selected variant of our method in Fig. 3. Specifically, we evaluate the generalized metric trained using the joint objective defined in (22). We systematically vary the miscoverage tolerance  $\alpha$ , the steepness of the sigmoid surrogate  $T$ , the contrastive loss weight  $\lambda_{\text{InfoNCE}}$ , the InfoNCE temperature  $\tau$ , the volume regularization constant  $\lambda$ , and the number of sampled instances  $k$ . Unless otherwise specified, the default parameters are  $\alpha = 0.05$ ,  $T = 7.0$ ,  $\lambda_{\text{InfoNCE}} = 1.0$ ,  $\tau = 0.1$ ,  $\lambda = 0.05$ , and  $k = 20$ .

As expected, increasing  $\alpha$  strictly decreases the target positive inclusion probability ( $1 - \alpha$ ), resulting in a linear decline in empirical coverage. Correspondingly, a larger  $\alpha$  yields a smaller quantile threshold  $\hat{q}_\alpha$ , shrinking the volume of the covering sets. Following Proposition 1, this reduced volume naturally translates to an increased negative exclusion rate. Across all other parameter sweeps, the empirical coverage remains stably bounded near 0.95, validating the distribution-free guarantee established in Lemma 1.

Modifying the steepness parameter  $T$  of the sigmoid approximation does not significantly impact the exclusion rate. While higher steepness values yield smaller volumes by more tightly approximating the hard indicator function, extreme values

Table 4: ImageNet-100, model=ResNet18,  $k = 20$ ,  $\alpha = 0.05$ ,  $n_{\text{test}} = 2500$ , seeds=3.

Method	Coverage	Exclusion	LogVol
Conformal Ball ( $\ell_2$ )	95.5 $\pm$ 0.1%	15.1 $\pm$ 0.1%	822.1 $\pm$ 0.3
Mahalanobis Ellipsoid	95.9 $\pm$ 0.1%	7.1 $\pm$ 0.2%	619.0 $\pm$ 0.2
Single (Vol)	92.5 $\pm$ 0.2%	27.7 $\pm$ 0.8%	1060.9 $\pm$ 2.8
Generalized (Vol)	93.2 $\pm$ 0.3%	36.3 $\pm$ 1.4%	467.3 $\pm$ 2.4
Single (Neg)	95.7 $\pm$ 0.2%	69.7 $\pm$ 0.6%	1962.0 $\pm$ 16.9
Generalized (Neg)	95.6 $\pm$ 0.3%	51.6 $\pm$ 1.0%	1090.1 $\pm$ 4.2
Single (Vol, InfoNCE)	93.0 $\pm$ 0.3%	27.9 $\pm$ 1.0%	-75.8 $\pm$ 55.0
Generalized (Vol, InfoNCE)	93.7 $\pm$ 0.4%	31.2 $\pm$ 0.7%	-1257.7 $\pm$ 83.5
Single (Neg, InfoNCE)	95.6 $\pm$ 0.2%	74.1 $\pm$ 0.3%	1642.8 $\pm$ 13.5
Generalized (Neg, InfoNCE)	96.1 $\pm$ 0.1%	72.4 $\pm$ 0.3%	656.5 $\pm$ 1.6
Single (Neg, Vol)	92.8 $\pm$ 0.4%	31.0 $\pm$ 0.5%	1071.6 $\pm$ 1.6
Generalized (Neg, Vol)	93.2 $\pm$ 0.1%	37.4 $\pm$ 0.4%	489.9 $\pm$ 2.1
Single (Neg, Vol, InfoNCE)	93.4 $\pm$ 0.4%	43.3 $\pm$ 1.2%	182.7 $\pm$ 48.2
Generalized (Neg, Vol, InfoNCE)	94.3 $\pm$ 1.0%	54.4 $\pm$ 3.7%	-1085.6 $\pm$ 44.9

Table 5: OOD detection on ImageNet-100 (ID). Backbone: ResNet18, seeds= 3.

Method	NINCO		TEXTURES	
	AUROC $\uparrow$	FPR95 $\downarrow$	AUROC $\uparrow$	FPR95 $\downarrow$
MSP	88.8 $\pm$ 0.1	38.0 $\pm$ 0.1	93.1 $\pm$ 0.1	27.3 $\pm$ 0.1
Energy ( $T=1$ )	89.9 $\pm$ 0.2	33.7 $\pm$ 0.3	90.2 $\pm$ 0.3	21.8 $\pm$ 0.7
Mahalanobis	71.7 $\pm$ 0.0	81.4 $\pm$ 0.0	84.5 $\pm$ 0.0	74.9 $\pm$ 0.0
KNN ( $\ell_2$ )	55.4 $\pm$ 0.5	88.3 $\pm$ 1.1	61.2 $\pm$ 0.9	84.1 $\pm$ 1.3
COMBOOD	89.5 $\pm$ 0.0	42.2 $\pm$ 0.0	98.7 $\pm$ 0.0	4.7 $\pm$ 0.0
D-KNN	87.6 $\pm$ 0.0	48.5 $\pm$ 0.0	99.1 $\pm$ 0.0	5.5 $\pm$ 0.0
CIDER	86.0 $\pm$ 0.4	45.6 $\pm$ 2.5	89.9 $\pm$ 0.4	32.3 $\pm$ 1.3
ViM	85.4 $\pm$ 0.0	48.3 $\pm$ 0.0	96.4 $\pm$ 0.0	17.1 $\pm$ 0.0
NAC	86.1 $\pm$ 0.0	52.8 $\pm$ 0.0	90.4 $\pm$ 0.0	42.0 $\pm$ 0.0
Generalized (Neg)	86.1 $\pm$ 0.6	75.5 $\pm$ 1.1	96.6 $\pm$ 0.2	15.2 $\pm$ 1.6
Single (Neg)	94.3 $\pm$ 0.1	49.8 $\pm$ 4.7	99.1 $\pm$ 0.1	0.3 $\pm$ 0.1
Generalized (Vol)	67.6 $\pm$ 1.3	90.5 $\pm$ 0.7	71.0 $\pm$ 0.9	98.2 $\pm$ 0.0
Single (Vol)	64.6 $\pm$ 1.4	90.9 $\pm$ 0.7	61.8 $\pm$ 0.6	97.4 $\pm$ 0.4
Single (Neg, Vol)	68.8 $\pm$ 1.5	89.3 $\pm$ 1.4	67.9 $\pm$ 2.3	96.2 $\pm$ 0.4
Generalized (Neg, Vol)	68.9 $\pm$ 0.5	90.0 $\pm$ 0.8	74.1 $\pm$ 1.1	97.7 $\pm$ 0.3
Single (Neg, InfoNCE)	96.9 $\pm$ 0.4	17.8 $\pm$ 3.2	99.3 $\pm$ 0.2	0.0 $\pm$ 0.1
Generalized (Neg, InfoNCE)	96.8 $\pm$ 0.0	19.0 $\pm$ 0.0	99.1 $\pm$ 0.1	0.0 $\pm$ 0.0
Single (Neg, Vol, InfoNCE)	80.0 $\pm$ 1.1	86.6 $\pm$ 0.5	77.3 $\pm$ 0.9	97.2 $\pm$ 0.3
Generalized (Neg, Vol, InfoNCE)	88.1 $\pm$ 1.3	76.0 $\pm$ 2.6	92.0 $\pm$ 1.1	73.6 $\pm$ 14.6

Table 6: OOD detection on STL10 (ID). Backbone: ResNet18-SimCLR, seeds= 3.

Method	SVHN		CIFAR10		CIFAR100		ImageNet100	
	AUROC $\uparrow$	FPR95 $\downarrow$						
MSP	72.1 $\pm$ 0.5	58.7 $\pm$ 1.0	71.8 $\pm$ 0.2	66.1 $\pm$ 0.2	69.8 $\pm$ 0.2	68.5 $\pm$ 0.1	72.5 $\pm$ 0.1	65.7 $\pm$ 0.4
Energy ( $T=1$ )	70.5 $\pm$ 1.4	57.8 $\pm$ 2.0	71.0 $\pm$ 0.5	65.2 $\pm$ 0.6	69.5 $\pm$ 0.5	68.4 $\pm$ 0.9	74.3 $\pm$ 0.4	63.7 $\pm$ 0.1
Mahalanobis	61.6 $\pm$ 0.0	76.2 $\pm$ 0.0	48.7 $\pm$ 0.0	89.5 $\pm$ 0.0	49.8 $\pm$ 0.0	88.2 $\pm$ 0.0	49.6 $\pm$ 0.0	92.2 $\pm$ 0.0
KNN ( $\ell_2$ )	57.9 $\pm$ 1.4	76.0 $\pm$ 2.1	57.7 $\pm$ 0.5	85.0 $\pm$ 0.4	54.2 $\pm$ 0.7	87.5 $\pm$ 0.9	57.2 $\pm$ 0.8	86.7 $\pm$ 0.9
COMBOOD	96.7 $\pm$ 0.0	17.8 $\pm$ 0.0	83.9 $\pm$ 0.0	50.0 $\pm$ 0.0	85.0 $\pm$ 0.0	49.3 $\pm$ 0.0	78.0 $\pm$ 0.0	58.1 $\pm$ 0.0
D-KNN	90.3 $\pm$ 0.0	29.9 $\pm$ 0.0	76.9 $\pm$ 0.0	56.2 $\pm$ 0.0	78.6 $\pm$ 0.0	53.7 $\pm$ 0.0	76.0 $\pm$ 0.0	59.6 $\pm$ 0.0
CIDER	83.2 $\pm$ 14.1	41.7 $\pm$ 30.2	83.9 $\pm$ 12.1	43.9 $\pm$ 31.3	66.2 $\pm$ 1.0	78.2 $\pm$ 2.7	70.1 $\pm$ 0.3	72.5 $\pm$ 1.7
Generalized (Neg)	99.8 $\pm$ 0.0	0.1 $\pm$ 0.1	98.3 $\pm$ 0.0	5.5 $\pm$ 1.0	98.6 $\pm$ 0.1	4.7 $\pm$ 1.2	98.4 $\pm$ 0.1	6.5 $\pm$ 0.4
Single (Neg)	98.7 $\pm$ 0.3	1.2 $\pm$ 1.2	92.0 $\pm$ 0.7	61.0 $\pm$ 5.9	93.3 $\pm$ 0.4	59.0 $\pm$ 1.5	93.7 $\pm$ 1.3	45.4 $\pm$ 9.5
Generalized (Neg, InfoNCE)	95.4 $\pm$ 0.7	31.1 $\pm$ 4.1	92.8 $\pm$ 0.7	39.8 $\pm$ 3.2	91.0 $\pm$ 0.8	49.4 $\pm$ 2.9	82.2 $\pm$ 1.7	79.3 $\pm$ 3.4

can induce vanishing gradients around the threshold boundary, potentially destabilizing optimization.

The coefficient  $\lambda_{\text{InfoNCE}}$  controls the influence of the contrastive loss. A stronger contrastive penalty enforces better semantic separation, leading to higher negative exclusion. However, the set volume fluctuates under this parameter: excessively high contrastive weights overshadow the volume regularization term in (22), resulting in larger volumes. Conversely, if  $\lambda_{\text{InfoNCE}}$  is too small, the encoder struggles to cluster positive samples tightly, forcing the conformal sets to expand to satisfy the required coverage level.

A higher InfoNCE temperature  $\tau$  sharpens the separation between positive and negative samples, directly improving the exclusion rate. On the other hand, increasing the volume regularization constant  $\lambda$  inherently reduces the relative weight of the negative exclusion term in  $J_{\text{neg+vol}}$ , yielding more compact sets but a slightly lower exclusion rate.

Finally, the exclusion rate demonstrates remarkably low sensitivity to the number of generated positive and negative samples,  $k$ . This suggests that our negative exclusion objective can be optimized efficiently using fewer samples without degrading the discriminative quality of the resulting sets.

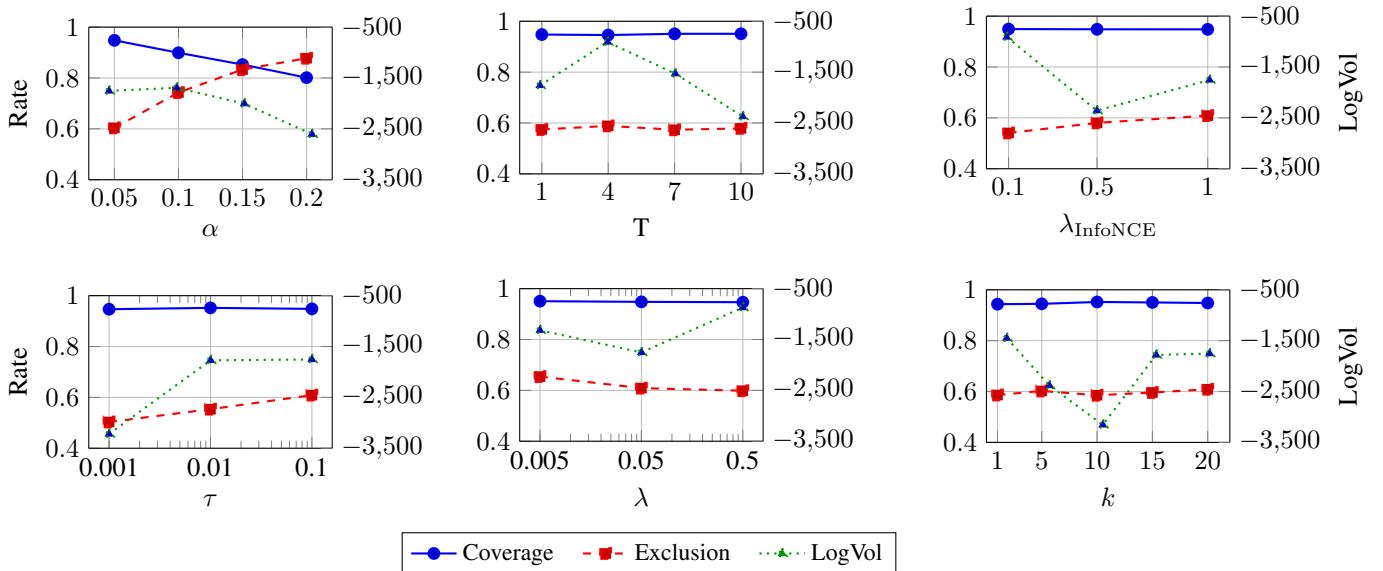


Figure 3: Sensitivity analysis results. (Top): Sweeping  $\alpha$ , steepness of sigmoid T, and  $\lambda_{\text{InfoNCE}}$ . (Bottom): Sweeping InfoNCE temperature  $\tau$ , regularization constant  $\lambda$ , and number of generated samples  $k$ . Coverage and Exclusion rates are plotted against the left axis, while Log Volume is plotted against the right axis.